Modeling frequency dependent scattering models for SAR Image Spectrum Extrapolation

Nithin Sugavanam, Emre Ertin

Department of Electrical and Computer Engineering,

The Ohio State University

Abstract—The wavelength used for illumination dictates the scale of the mechanisms that interact with the incident electromagnetic (EM) energy. We model the synthetic Aperture Radar Image of a target as a superposition of the returns from scattering mechanisms that depend on the wavelength of the illuminating waveform and the viewing angle. In this work, we present a method to jointly model the scattering responses of the target over a wide aperture of measurements and a wide swath of frequencies spanning the C to X Band. Specifically, we estimate the location of the scattering centers and their azimuth-dependent responses normalized by the wavelength, jointly for low and high bands. We verify the validity of the proposed model using simulated data from a backhoe and Civilian vehicle data domes dataset over two non-overlapping frequency bands centered at 7GHz and 12 GHz.

Index Terms—Frequency band extrapolation, dataaugmentation, wide-band scattering model

I. INTRODUCTION

This paper presents a method to learn compressed models for complex targets, such that phase-history measurements from a synthetic aperture radar (SAR) sensor can be synthesized for a desired frequency band. The compressed model of the target includes the spatial locations of the scattering centers and their view-dependent scattering coefficients and is estimated using the measurements from two disjoint frequency bands of fixed bandwidth. SAR imaging achieves high crossrange resolution as compared to real aperture radar [1]-[3] by integrating over a larger aperture. The integration over the azimuth domain increases the cross-range resolution but is constrained by the limited persistence of the scattering mechanism [4] as a function of the viewing angle. Alternatively, the scattering coefficients exhibit anisotropic behavior because of the monostatic geometry of the radar collection and the limited persistence of the scattering mechanism over a wideangle aperture [4]–[6].

Furthermore, the scattering behavior of the target depends on the wavelength of the illuminating waveform. The wavelength determines the minimum scale of the scattering mechanism that interacts with the electromagnetic energy. The cross-range resolution is directly proportional to the wavelength corresponding to the band's center frequency. At higher frequency bands, finer scattering mechanisms are prominent; therefore, the scattering center's persistence reduces as the band's center frequency increases. The scattering coefficients exhibit anisotropic scattering in the azimuth-angle and the

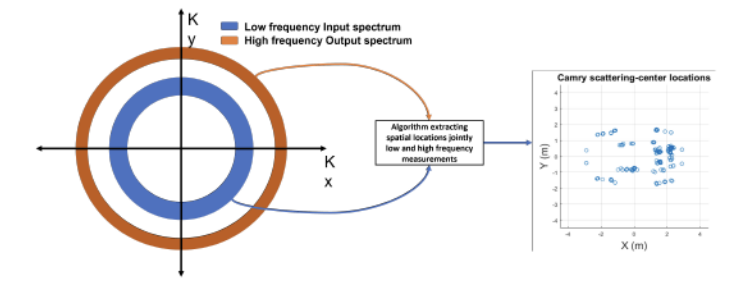


Fig. 1: Estimating a joint model over different frequency bands $F_1 = [7GHz, 7.64GHz]$ and $F_2 = [12GHz, 12.64GHz]$.

frequency domain [5], [7]. We hypothesize that the scattering response of an object at a waveform with the center frequency F_i is equivalent to the scattering response of the scaled object with a factor of S illuminated with a waveform with a center frequency $\frac{F_i}{S}$. This setup is particularly useful in simulating the scattering behavior of complex targets using scaled-down models with 0 < S < 1 at higher frequencies [8] in a compact range. The measurement setup can be miniaturized by utilizing millimeter wave radar, which enables the collection of measurements on scaled-down target models.

A. Contributions

We present a model that represents the wideband scattering behavior of a complex target over the entire circular azimuth aperture. This representation succinctly captures the scattering mechanism as a function of the viewing angle and center frequency. We formulate a regularized inversion approach to jointly estimate the scattering center locations and coefficients over disjoint frequency bands.

B. Notations

The observed frequency bands that are used to estimate the model are F_L and F_H with center frequencies denoted by f_L and f_H , respectively. The center frequencies of the bands where the model is evaluated and used for validation are denoted by F_i such that $f_L < F_i < f_H$. The bandwidth of the illuminating signals are B Hz. The azimuth angles observed over N_P pulses across the circular aperture is denoted by $\Theta = \theta_1, \theta_2, \cdots, \theta_{N_P}$ and the elevation angle is denoted by ϕ and the N_f frequency samples in the band centered at F_L

are denoted by $f_1^L, f_2^L, \cdots, f_{N_F}^L$ and the frequency samples centered around F_H are denoted by $f_1^H, f_2^H, \cdots, f_{N_F}^H$.

C. Related Work

Azimuth dependent parametric models for scattering centers have been proposed in [6], [9], [10] that utilize the persistence of these scattering centers in the azimuth domain. Frequency dependent models inspired from geometric theory of diffraction have been proposed in [11], [12]. We previously proposed regularization based approaches for imaging in 2D and 3D for monostatic [4], [13], [14], and bistatic SAR [15], [15], [16]. The frequency extrapolation problem has recently been analyzed using Generative adversarial network for the case of missing frequency band measurements due to interference [17], [18].

II. SEMI-PARAMETRIC MODEL AND REGULARIZED INVERSION

We consider a circular spotlight SAR setup in a monostatic transmit and receive geometry. We specifically consider two bands of frequencies F_L and F_H centered at f_L and f_H with bandwidth B Hz. The phase history measurements obtained through stretch processing is modeled in the K-space domain. The measurements are collected over different frequencies, azimuth and elevation angles. We denote these measurements by $\mathbf{Y}(f,\theta,\phi)\in\mathbb{C}^{2N_F\times N_P}$, where the frequencies $f=[f_1^L,\cdots,f_{N_F}^L,F_1^H,\cdots,F_{N_F}^H]$, azimuth angles $\Theta=\theta_1,\cdots,\theta_{N_P}$, and elevation angles $\Phi=\phi_1,\cdots,\phi_{N_P}$. The scattering coefficients of the scene is assumed to be anisotropic as a function of azimuth angle and the wavelength corresponding to the center-frequency of the band as shown below

$$Y(f,\theta,\phi) = \int_{x,y,z} g(x,y,z,\theta,f) \times \exp\left(-j\left(xK_x + yK_y + zK_z\right)\right) dxdydz.$$
 (1)

The K-space spatial frequencies are a function of the azimuth angle θ , illumination frequency f and elevation angle ϕ as shown below

$$K_{x} = \frac{4\pi f}{c} \cos(\theta) \sin(\phi),$$

$$K_{y} = \frac{4\pi f}{c} \sin(\theta) \sin(\phi),$$

$$K_{z} = \frac{4\pi f}{c} \cos(\phi).$$

Classical methods solve the imaging problem using regularization based optimization method [19] and the reconstruction is made tractable by considering overlapping or non-overlapping sub-apertures with constant scattering coefficients. The slant-range resolution is given by $\Delta R = \frac{c}{2B}$, where c is the velocity of light and B is the bandwidth of the transmitted signal. The unambiguous range is given by $R_u = \frac{c}{2\Delta f}$, where Δ_f is the difference between successive frequency samples. The cross-range resolution under the assumption of a narrow-band signal compared to the center-frequency is given by $\Delta C_r = \frac{\lambda}{2\Delta\Theta}$,

where λ is the wavelength corresponding to the center frequency and $\Delta\Theta$ is the span of the azimuth angles considered in the sub-aperture. We consider two disjoint frequency bands $F_L = [7GHz, 7.64GHz]$ and $F_H = [12GHz, 12.64GHz]$ as shown in Figure 1.

We propose to recover the scattering coefficients of the scene over the entire azimuth aperture and frequency bands. We hypothesize that the object comprises of a sparse set of dominant scattering centers with smooth azimuth and frequency dependent scattering coefficients. We approximate the scattering coefficients function $g(x, y, \theta, f)$ described in (1) using a set of Gaussian basis functions based on the previous work [20]–[22]. We observe that the cross-range resolution is proportional to the wavelength of the band corresponding to the center-frequency. Using this observation, we hypothesize that as the center-frequency of the illuminating waveform increases the persistence of the scattering mechanism starts reducing because finer details of the scattering behavior start dominating. The scattering coefficient at a location with coordinates (x_i, y_i) is approximated using a set of Gaussian basis functions and a frequency-dependent scaling function $\left(j\frac{f}{f_L}\right)^{\alpha_i}$ if $f\in F_L$ or $\left(j\frac{f}{f_H}\right)^{\alpha_i}$ if $f\in F_H$. $c_i(f_L)\in\mathbb{C}$ and $c_i(f_H)\in\mathbb{C}$ represents the complex weighing coefficients estimated at bands F_L and F_H , respectively and \hat{n} represents the modeling error. The approximation of the scattering coefficients are given by

$$g(x, y, \theta, f; f_c) = \sum_{k=1}^{K} c_k(f_c) \bar{\Psi}(x_k, y_k, \mu_k, \sigma_k, \theta, f; f_c) + \hat{n}$$
(2)

$$\bar{\Psi}(x_k, y_k, \mu_k, \sigma_k, \theta, f; f_c) = \delta(x - x_k, y - y_k) \times \left(j\frac{f}{f_c}\right)^{\alpha} \exp\left(\frac{-\left(\theta - \mu_k\right)^2}{2\left(\frac{\sigma_k}{c/f_c}\right)^2}\right), \tag{3}$$

where $f_c \in \{f_L, f_H\}$, K denotes the number of dominant scattering centers, $\bar{\Psi}(x_k, y_k, \mu_k, \sigma_k, \theta, f; f_c)$ denotes the approximation of the scattering coefficient that is decomposed into a function that depends on the spatial location (x_k, y_k) , illumination frequency f and the azimuth angle. We decouple the frequency dependent scattering behavior as two components. The first component is encoded in the complex weight for each scattering center and the second component encodes the effect of the increased frequency on the persistence of the scattering center by scaling the width of the Gaussian basis function with the center frequency of the illuminating band. This decoupling leads to a common set of parameters denoted by $\{X, Y, \mu, \sigma, \alpha\}$ independent of the center frequency that represent the complex target and a frequency dependent scaling coefficient $C(f_c) = [c_1(f_c), c_2(f_c), \cdots, c_K(f_c)] \in \mathbb{C}^K$. The set consisting of the coordinate locations of scattering centers is give by $(X,Y) = \{(x_1,y_1), (x_2,y_2), \cdots, (x_K,y_K)\}.$ The set of Gaussian window centers and widths to model the azimuth dependent function is given by $\mu = [\mu_1, \mu_2, \cdots, \mu_K]$

and $\sigma = [\sigma_1, \sigma_2, \cdots, \sigma_K]$. The effect of lower persistence in the azimuth domain as the wavelength increases is modeled as a reduction in the width parameter of the Gaussian basis given by $\frac{\sigma_k}{c/f_c}$. The phase-history measurements can be reformulated as follows

$$\mathbf{Y}(f_c) = \sum_{k=1}^{K} c_k(f_c) \Psi(x_k, y_k, \mu_k, \sigma_k; f_c) + \mathbf{n},$$
 (4)

$$\Psi\left(x_{k}, y_{k}, \mu_{k}, \sigma_{k}; f_{c}\right) = \exp\left(-j\left(\mathbf{K}_{\mathbf{x}} x_{k} + \mathbf{K}_{\mathbf{y}} y_{k}\right)\right) \times$$

$$\left(j\frac{\mathbf{F}}{f_c}\right)^{\alpha} \exp\left(\frac{-\left(\theta - \mu_k\right)^2}{2\left(\frac{f_c\sigma_k}{c}\right)^2}\right),$$
 (5)

where K_x , K_y are the spatial frequencies evaluated for all the observed frequencies and azimuth angles. The inverse problem for jointly estimating the scattering center locations and the azimuth and frequency dependent scattering parameters can be written as

$$\min_{c,x,y,\mu,\sigma,\alpha} \sum_{f_c} \|\mathbf{Y}(f_c) - \sum_{k=1}^{K} c_k(f_c) \Psi(x_k, y_k, \mu_k, \sigma_k; f_c)\|_2^2 + \lambda \|c\|_1$$
(6)

We utilize the differentiability of the proposed parametrization and solve the regularized inverse problem in the continuum using alternating descent conditional gradient method proposed by Recht [23]. We denote the search space of the center frequency independent parameters given by $\{x,y,\mu,\sigma,\alpha\}\in\Omega$. We elaborate the method in Algorithm 1. The advantage of decoupling the parameter sets $\{X,Y,\mu,\sigma,\alpha\}$ and $\{C(f_c)\}$ is that the fixed parameters independent of f_c can be estimated once using the given observations in the frequency band F_L and F_H . We estimate the coefficients $C(f_i)$ for a new frequency bands f_i while using the same parameter set $\{X,Y,\mu,\sigma,\alpha\}$. Given the phase-history measurements $Y(f_i)$ at a frequency band with center frequency f_i , we solve the problem

$$C^*(f_i) = \arg \min_{c(f_i)} \|\mathbf{Y}(f_i) - \sum_{k=1}^{K} c_k(f_i) \Psi(x_k, y_k, \mu_k, \sigma_k; f_i)\|_2^2.$$
(9)

In the next section, we apply and validate the proposed model and algorithm on monostatic SAR measurements.

III. EXPERIMENTS

We utilize the Backhoe dataset and the simulated dataset Civilian vehicle radar data domes [24] to evaluate the performance of our modeling approach in the different frequency bands. The parameters used in the experiments are detailed in Table I. The measurements are obtained at azimuth angles [0, 360] degrees at a spacing of 0.0625 degree spacing between successive pulses. The bandwidth used to illuminate the scene is 640 MHz, and the corresponding range resolution is 0.22 m. We apply the algorithm 1 to extract the estimate the model parameters to represent the target using phase-history

Input: $\mathbf{Y}, \mathbf{\tau}, \mathbf{\Psi}, \nabla_{\{x,y,\mu,\sigma,\alpha\} \in \Omega} \mathbf{\Psi}, \Omega$, and K_{max} . Return: complex weights \mathbf{c} , spatial location of scattering centers, mean and width of the Gaussian basis function $\{x,y,\mu,\sigma,\alpha\} \in \Omega$. Initialize k=0, support set $S=\{\emptyset\}$ while (Convergence condition is not satisfied or $k \leq K_{max}$)

Residual: $\mathbf{r}_k(f_c) = \mathbf{Y}(\mathbf{f_c}) - \sum_{k=1}^{k-1} \mathbf{\Psi}(x_k,y_k,\mu_k,\sigma_k,\theta,f;f_c)\,c_k(f_c)$, (7)

Gradient of loss function: $\mathbf{g}_k(\mathbf{r}_k) = \nabla_{\mathbf{r}}\left(0.5\sum_{f_c}\|\mathbf{r}_k(f_c)\|_2^2\right)$ $\{x_k,y_k,\mu_k,\sigma_k,\alpha_k\} =$ $\mathbf{g}_{\{x,y,\mu,\sigma,\alpha\} \in \Omega} |\langle \mathbf{\Psi}(x_k,y_k,\mu_k,\sigma_k,\alpha_k,f),\mathbf{g}_k \rangle|,$ $S=S\bigcup \{x_k,y_k,\mu_k,\sigma_k,\alpha_k\}$ while (Convergence condition)

Compute weights: $\underset{\|\mathbf{c}(f_c)\|_1 \leq \tau}{\min} \|\mathbf{\Psi}(f_c)\mathbf{c}(f_c) - \mathbf{Y}(f_c)\|^2$ $\underset{\|\mathbf{c}(f_c)\|_1 \leq \tau}{\|\mathbf{c}(f_c)\|_1 \leq \tau}$ Prune Support: If $|c_k(f_c)| = 0$ $S=S\setminus \{x_k,y_k,\mu_k,\sigma_k,\alpha_k\}$ Refine support: $S=S-\nabla_S\left(\sum_{f_c}\|\mathbf{\Psi}(f_c)\mathbf{c}(f_c) - \mathbf{Y}(f_c)\|^2\right)$ end S=S

Algorithm 1: Alternating descent conditional gradient method for 2D SAR imaging with frequency dependent model [23]

TABLE I: Parameter setup.

Parameter	Value		
Bandwidth	640 MHz		
Azimuth Angle in sub-aperture	3.1 to 5 degrees across center		
	frequencies		
Azimuth angle range Backhoe	-10 to 105 degrees		
Azimuth angle range Civilian	0 to 360 degrees		
domes	· ·		
$\Delta heta$	0.0625 degrees		
Unambiguous Range and	14.3 m		
Cross-range			
Center Frequencies Train	7GHz, 12GHz		
Center Frequencies Test	8, 9, 10, 11GHz		

measurements centered over frequency bands F_L and F_H . Using the parameters $\{X, Y, \mu, \sigma, \alpha\}$ estimated over F_H and F_L , we estimate the complex weights over other frequency bands f_i . In the next section, we reconstruct the Backhoe and Civilian vehicle data-domes over the frequencies $f_i = \{7, 8, 9, 10, 11, 12\}GHz$ by solving the problem described in (9).

IV. RESULTS

We evaluated the proposed frequency-dependent model on the Civilian data domes and Backhoe dataset. We estimated the joint model for each target using measurements in 7GHz and 12GHz. We evaluated the model's performance operating on newer bands not utilized in the estimation process. The coefficients c(fc) are re-estimated using Least squares in this current work. Table II gives the normalized mean squared error. The normalized mean square error increases with frequency bands $f_i = 8, 8, 10, 11$ GHz is higher than $f_i = 7, 12$ GHz because the fixed parameter set was estimated for those frequencies. This observation suggests that the persistence model has a more complicated relationship than the linear scaling used in the proposed semi-parametric model.

Next, we present the scattering coefficient as a function of the azimuth angle and the center frequency band for the backhoe dataset in Figure 2. We see that the model can predict the scattering behavior over frequency bands $f_i = 7, 8, 9, 10, 11, 12$ GHz and captures the reduction in the persistence of scattering centers in the azimuth angle domain as the center frequency increases. The ground-truth scattering coefficients are computed using back-projected images evaluated using sub-aperture approximation.

Next, we evaluate the behavior of the estimated model as a function of the center frequency. We find the dominant 5 scattering centers from 7 GHz data and track the variation of the weights across different center frequencies, as shown in Figure 3. The magnitude is stable with a decreasing trend, and the phase also exhibits a linear ramp behavior. We plan to exploit this structure to perform prediction in a sequel to this work.

V. CONCLUSION

In this work, we presented a joint model for recovering scattering center locations and the reflection coefficients as a function of azimuth angle and center frequency. We provided quantitative validation of the proposed modeling approach and parameter estimation algorithm. In our future work, we propose further solving the problem of predicting the frequencydependent scattering mechanism using data-driven methods.

REFERENCES

- [1] N. Sugavanam, S. Baskar, and E. Ertin, "High resolution radar sensing
- with compressive illumination," arXiv preprint arXiv:2106.11490, 2021.
 [2] N. Sugavanam and E. Ertin, "Recovery guarantees for MIMO radar using multi-frequency LFM waveform," in 2016 IEEE Radar Conference (RadarConf). IEEE, 2016, pp. 1-6.
- [3] N. Sugavanam, S. Baskar, and E. Ertin, "High resolution mimo radar sensing with compressive illuminations," IEEE Transactions on Signal Processing, vol. 70, pp. 1448-1463, 2022.
- [4] N. Sugavanam and E. Ertin, "Limited persistence models for sar automatic target recognition," in Algorithms for Synthetic Aperture Radar Imagery XXIV, vol. 10201. SPIE, 2017, pp. 105-116.
- [5] R. L. Moses, L. C. Potter, and M. Cetin, "Wide-angle SAR imaging," Proc. SPIE, Algorithms for Synthetic Aperture Radar Imagery XI, vol. 5427, pp. 164-175, 2004.
- [6] K. R. Varshney, M. Cetin, J. W. Fisher III, and A. S. Willsky, "Joint image formation and anisotropy characterization in wide-angle SAR, Proc. SPIE Algorithms for Synthetic Aperture Radar Imagery XIII, vol. 6237, pp. 62370D-62370D-12, 2006.
- [7] L. C. Potter, D.-M. Chiang, R. Carriere, and M. J. Gerry, "A GTD-based parametric model for radar scattering," IEEE Transactions on Antennas and Propagation, vol. 43, no. 10, pp. 1058–1067, 1995.
- C. Beaudoin, A. Gatesman, M. Clinard, J. Waldman, R. Giles, and W. Nixon, "Physical scale modeling of VHF/UHF SAR collection geometries," in Proceedings of the 2004 IEEE Radar Conference (IEEE Cat. No. 04CH37509). IEEE, 2004, pp. 508-513.
- [9] J. A. Jackson, B. D. Rigling, and R. L. Moses, "Canonical scattering feature models for 3D and bistatic SAR," IEEE Transactions on Aerospace and Electronic Systems, vol. 46, no. 2, pp. 525-541, 2010.

- [10] —, "Parametric scattering models for bistatic synthetic aperture radar," in 2008 IEEE Radar Conference. IEEE, 2008, pp. 1-5.
- [11] L. C. Potter and R. L. Moses, "Attributed scattering centers for SAR ATR," IEEE Transactions on image processing, vol. 6, no. 1, pp. 79-91, 1997.
- [12] M. J. Gerry, L. C. Potter, I. J. Gupta, and A. Van Der Merwe, "A parametric model for synthetic aperture radar measurements," IEEE transactions on antennas and propagation, vol. 47, no. 7, pp. 1179-1188, 1999.
- [13] N. Sugavanam and E. Ertin, "Interrupted SAR imaging with limited persistence scattering models," in 2017 IEEE Radar Conference (Radar-Conf). IEEE, 2017, pp. 1770-1775.
- -, "Models of anisotropic scattering for 3D SAR reconstruction," in 2022 IEEE Radar Conference (RadarConf22). IEEE, 2022, pp. 1-6.
- [15] N. Sugavanam, E. Ertin, and R. Burkholder, "Approximating bistatic SAR target signatures with sparse limited persistence scattering models," in Int. Conf. on Radar, Brisbane, 2018.
- -, "Compressing bistatic sar target signatures with sparse-limited persistence scattering models," IET Radar, Sonar & Navigation, vol. 13, no. 9, pp. 1411-1420, 2019.
- [17] A. A. Nair, A. Rangamani, L. H. Nguyen, M. A. L. Bell, and T. D. Tran, "Spectral gap extrapolation and radio frequency interference suppression using 1D UNets," in 2021 IEEE Radar Conference (RadarConf21). IEEE, 2021, pp. 1–6.
- [18] L. Nguyen, D. N. Tran, and T. D. Tran, "Spectral gaps extrapolation for stepped-frequency SAR via generative adversarial networks," in 2019 IEEE Radar Conference (RadarConf). IEEE, 2019, pp. 1-6.
- [19] L. C. Potter, E. Ertin, J. T. Parker, and M. Cetin, "Sparsity and compressed sensing in radar imaging," Proceedings of the IEEE, vol. 98, no. 6, pp. 1006-1020, 2010.
- [20] L. C. Trintinalia, R. Bhalla, and H. Ling, "Scattering center parameterization of wide-angle backscattered data using adaptive Gaussian representation," IEEE Transactions on Antennas and Propagation, vol. 45, no. 11, pp. 1664-1668, Nov 1997.
- [21] L. C. Trintinalia and H. Ling, "Joint time-frequency ISAR using adaptive processing," IEEE Transactions on Antennas and Propagation, vol. 45, no. 2, pp. 221–227, Feb 1997.
- [22] S. Qian and D. Chen, "Signal representation using adaptive normalized
- gaussian functions," Signal Processing, vol. 36, no. 1, pp. 1 11, 1994. [23] N. Boyd, G. Schiebinger, and B. Recht, "The alternating descent conditional gradient method for sparse inverse problems," SIAM Journal on Optimization, vol. 27, no. 2, pp. 616-639, 2017.
- [24] K. E. Dungan, C. Austin, J. Nehrbass, and L. C. Potter, "Civilian vehicle radar data domes," in Algorithms for synthetic aperture radar Imagery XVII, vol. 7699. International Society for Optics and Photonics, 2010, p. 76990P.

TABLE II: Performance evaluation.

Vehicle	Normalized MSE					
	at 7GHz	at 8GHz	at 9GHz	at 10GHz	at 11GHz	at 12GHz
Backhoe	0.0883	0.1009	0.13	0.16	0.16	0.1422
Camry	0.3522	0.4021	0.377	0.3911	0.3976	0.3893
Maxima	0.3	0.328	0.382	0.348	0.36	0.34
Mitsubishi	0.309	0.36	0.44	0.48	0.45	0.42
Toyota Avalon	0.19	0.21	0.19	0.22	0.25	0.28
Toyota Tacoma	0.31	0.37	0.4	0.41	0.41	0.46

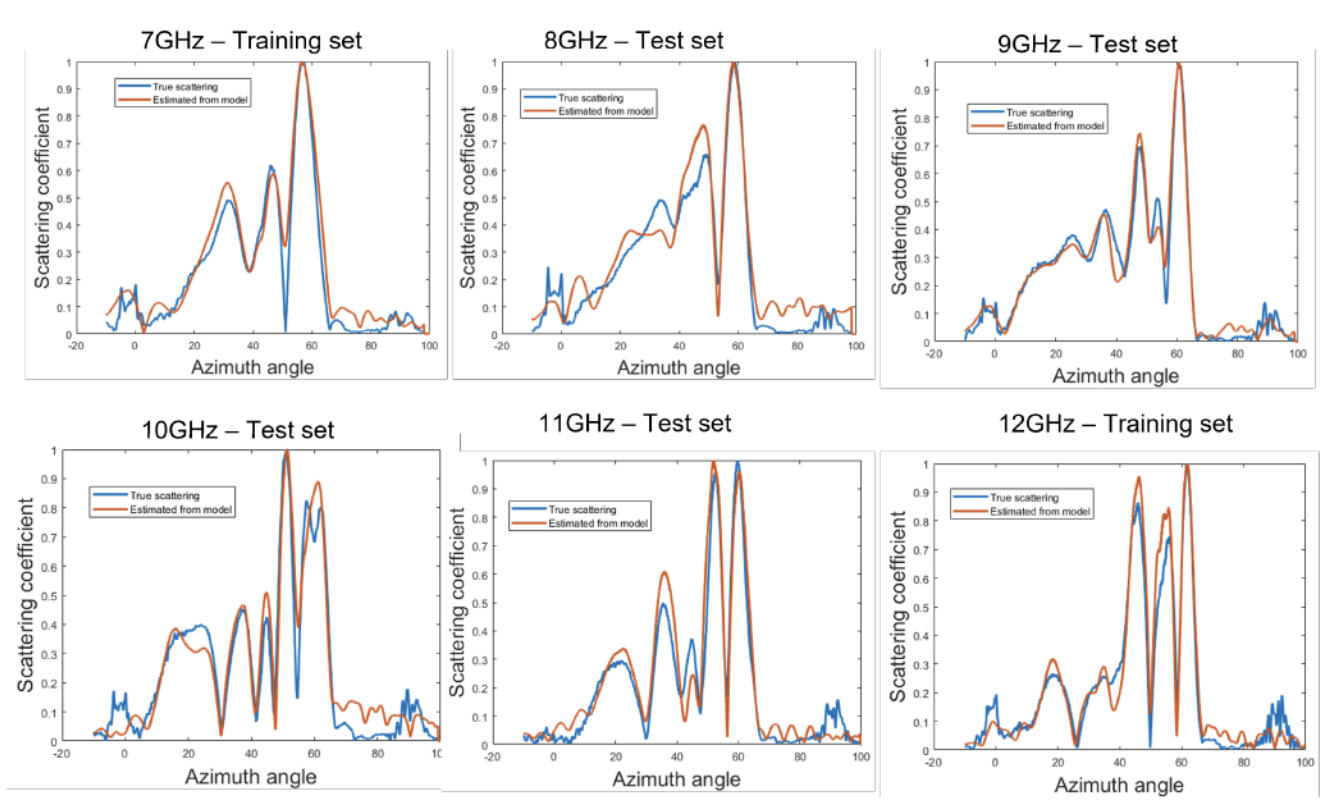


Fig. 2: Estimating a joint model for Backhoe over different frequency bands $F_1=[7GHz,7.64GHz]$ and $F_2=[12GHz,12.64GHz]$. The scattering coefficients are estimated over $F_c=8GHz,9GHz,10GHz$ and $T_c=12GHz$.

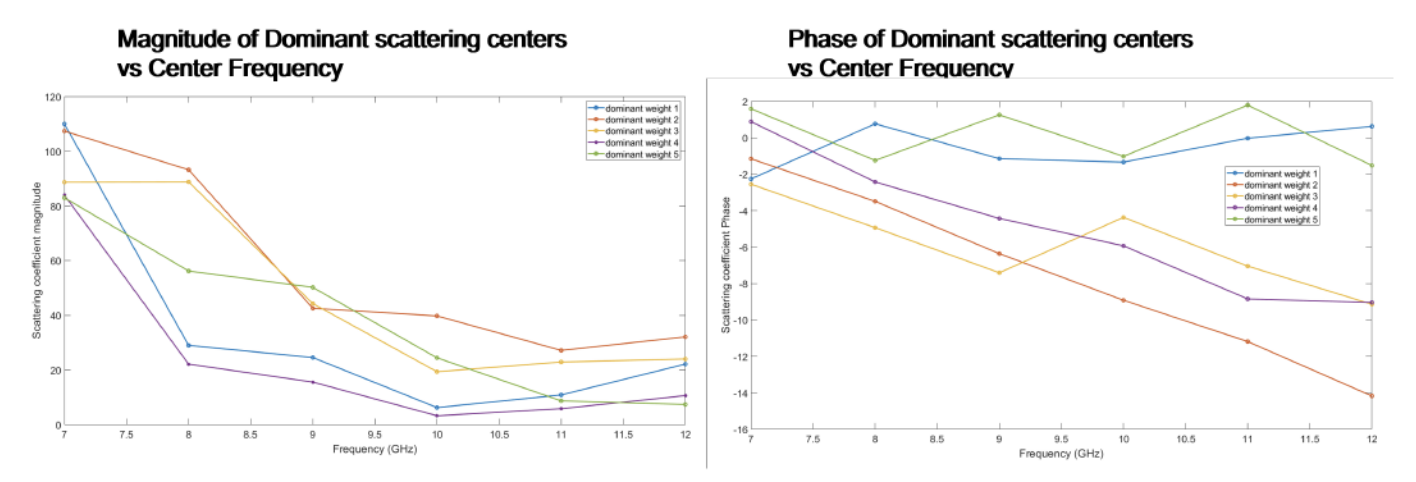


Fig. 3: The magnitude and phase of the dominant scattering centers estimated from the model as a function of the center Frequency is shown.